A Novel Hepatic-Targeting System for Therapeutic Cytokines That Delivers to the Hepatic Asialoglycoprotein Receptor, but Avoids Receptor-Mediated Endocytosis

Haruya Sato,[1] Yukio Kato,[1,2] Eiko Hayashi,[1] Tomoyuki Tabata,[1] Manabu Suzuki,[1] Yoshiyuki Takahara,[1] and Yuichi Sugiyama[1,2,3]

Received June 27, 2002; accepted August 5, 2002

Purpose. To demonstrate the utilities of a synthetic low-affinity ligand ($(Gal)_3$) for the asialoglycoprotein receptor (ASGP-R) as a hepatic targeting device for therapeutic cytokines.

Methods. The site-specific incorporation of $(Gal)_3$ or a typical high-affinity ligand $(GalNAc)_3$ into IL-2 was catalyzed by microbial transglutaminase. The anti-tumor activities, pharmacokinetic profiles and receptor-mediated endocytosis in hepatocytes of the ligand-IL-2 conjugates were examined in mouse.

Results. The $(Gal)_3$ has approximately 50 times lower affinity to ASGP-R than $(GalNAc)_3$. Nevertheless, the antitumor effects were in the order of $(Gal)_3$—IL-2 > unmodified IL-2 > $(GalNAc)_3$—IL-2. The systemic elimination and the hepatic uptake of $(GalNAc)_3$—IL-2 were more rapid than $(Gal)_3$—IL-2. The ratio of the rate constant representing dissociation from the cell-surface receptor (k_{off}) to that representing endocytosis of the ligand (k_{int}) was greater for $(Gal)_3$—IL-2 than $(GalNAc)_3$—IL-2, suggesting that $(Gal)_3$—IL-2 preferably avoids internalization due to its lower affinity to the receptor. The simulation studies demonstrated that $(Gal)_3$—IL-2 was present in the hepatic extracellular space for a longer period than $(GalNAc)_3$ IL-2.

Conclusions. The $(Gal)_3$ ligand increases the therapeutic efficacy of IL-2 by enhancing its exposure to the cell-surface. The k_{off}/k_{int} affects the targeting efficacy of the conjugates to ASGP-R.

KEY WORDS: interleukin 2; low-affinity ligand; galactose; transglutaminase; hepatic tumor; physiologically-based pharmacokinetic model.

INTRODUCTION

Many types of endogenous proteins, such as cytokines, are produced and released to act locally in the body, thus exerting the desired activity among their multiple functions. Hence, the exogenous administration of such proteins into the systemic circulation may result in undesired toxicological activities due to their low targeting efficiencies to the site of action. This could be one of the stumbling blocks that hinder their clinical application, and the specific delivery of the proteins to the action site would be necessary to overcome such problems.

Mammalian liver cells possess a specific membrane bound receptor for glycoproteins containing terminal galactose (Gal) or N-acethylgalactosamine (GalNAc) residues, the asialoglycoprotein receptor (ASGP-R) (1,2). Glycoprotein uptake by this receptor is both a high-affinity and high-capacity process (3,4). These features, combined with its specific localization on hepatocytes, make it an attractive target for mediating a specific delivery of drugs and genes to this metabolically important cell. There also have been some reports describing the targeting of proteins to the liver via ASGP-R by incorporating Gal residues into the protein molecules or constructing the asialoproteins, in which the sialic acids were removed from the N-linked oligosaccharide chain (5,6). Although those approaches have achieved highly specific targeting of the proteins to hepatocytes, their therapeutic efficiency was not always improved, possibly due to the ASGP-R-mediated endocytosis and the subsequent intracellular degradation of the proteins.

To overcome this problem, more detailed pharmacokinetic studies for other types of ASGP-R ligands are needed to optimize both the affinity to the receptor and the efficacy of endocytosis, since higher affinity of ASGP-R ligands may cause higher efficiency of endocytosis. We have developed a novel hepatic targeting system for proteins by utilizing an artificial ligand (named $(Gal)_3$) for ASGP-R (7). In our previous studies, $(Gal)_3$-incorporated IL-2 ($(Gal)_3$—IL-2) accumulated in the liver 2 min after i.v. administration in mice. High homogeneity (incorporation site: Gln74) and the increased hepatic distribution of the $(Gal)_3$—IL-2 may increase the therapeutic efficacy of IL-2 in hepatic tumor treatment.

We report herein pharmacological activity and pharmacokinetic property of a novel hepatic-targeting system, which delivers therapeutic cytokines to the hepatic ASGP-R by utilizing $(Gal)_3$. To demonstrate the utility of the $(Gal)_3$ ligand, we compared the therapeutic efficiencies and the disposition profiles in hepatocytes of $(Gal)_3$—IL-2 and $(GalNAc)_3$-incorporated IL-2 ($(GalNAc)_3$—IL-2), which is a typical high-affinity ligand for ASGP-R. We also performed a simulation study based on a physiologically-based pharmacokinetic (PBPK) model to demonstrate the optimized kinetic properties regarding the binding and subsequent internalization of the ligand via ASGP-R, in order to deliver IL-2 efficiently to the liver.

MATERIALS AND METHODS

Materials

M-TGase was purified from the culture supernatant of *Streptoverticillium sp.* S-8112 as described previously (7). IL-2 was purified from inclusion bodies, as described by Tsuji *et al.* (8). Asialoorosomucoid (ASOR) was prepared by desialylation of orosomucoid according to the method of Bider *et al.* (9). Other chemicals were of reagent grade.

Synthesis of $(GalNAc)_3$

The $(GalNAc)_3$ has three N-acetylgalactosamine residues in place of the galactose residues on the triantennary

[1] Pharmaceutical Research Laboratories, Ajinomoto Co., Inc. Suzuki-cho, Kawasaki-ku, 210-8681 Japan.
[2] Graduate School of Pharmaceutical Sciences, University of Tokyo, 7-3-1 Hongo, Bunkyo-ku, Tokyo 113-0033, Japan.
[3] To whom correspondence should be addressed at Graduate School of Pharmaceutical Sciences, University of Tokyo, 7-3-1 Hongo, Bunkyo-ku, Tokyo 113-0033, Japan. (e-mail: sugiyama@mol.f.u-tokyo.ac.jp)

0724-8741/02/1100-1736/0 © 2002 Plenum Publishing Corporation

structure in $(Gal)_3$. The synthesis of $(GalNAc)_3$ was carried out according to the modified method for $(Gal)_3$ (10). $(GalNAc)_3$; ESI + QIMS: m/z $(M + H)^+$ 1393.1. The purity of the $(GalNAc)_3$ was more than 95%, as analyzed by RP-HPLC with an Inertsil ODS-2 column (4.6 × 150 mm; GL Science Inc., Tokyo, Japan), which was developed by a linear gradient of 4–20% acetonitrile containing 0.1% TFA for 30 min at a flow rate of 1 ml/min, as described previously (7).

Conjugation, Purification, and Radioiodination of the Protein Samples

The conjugation of $(Gal)_3$ and $(GalNAc)_3$ to IL-2 was performed by M-TGase as described previously (7). To exclude endotoxin and other contaminants, unmodified IL-2, $(Gal)_3$—IL-2, and $(GalNAc)_3$—IL-2 were purified by RP-HPLC (YMC-C8AP column, YMC Inc. Kyoto, Japan) and gel-filtration chromatography (Sephadex G25 column, Amersham Pharmacia Biotech Inc., Piscataway, NJ USA). The specific activities of $(Gal)_3$—IL-2 and $(GalNAc)_3$—IL-2 were determined by IL-2 biological assays using the Gillis' method (11). The radioiodinations of ASOR, $(Gal)_3$—IL-2, and $(GalNAc)_3$—IL-2 were performed by the chloramine T method (12) using $Na^{125}I$ (Amersham Pharmacia Biotech Inc., Piscataway, NJ USA). The specific radioactivities of ^{125}I-ASOR, $(Gal)_3$—IL-2, and $(GalNAc)_3$—IL-2 were 9.5×10^6, 6.9×10^6 and 2.0×10^6 cpm/μg, respectively, and each labeled protein was >90% precipitable by 10% trichloroacetic acid (TCA).

Pharamacokinetics of Ligand—IL-2 Conjugates

The plasma concentration and the liver accumulation profiles in male mice (C57BL/6, 6w, Charles River Japan Inc., Sagamihara, Japan) were determined by ELISA (Cayman Chemical Co., Michigan, MI USA) after i.v. administration of IL-2, $(Gal)_3$—IL-2, and $(GalNAc)_3$—IL-2 (50 μg as IL-2/kg). Tissue uptake clearance (CL_{uptake}) was assessed as the amount of radioactivity in tissue at 3 min divided by the area under the plasma concentration profile (AUC) of the TCA-precipitable radioactivity from 0 to 3 min after intravenous administration (50 μg of IL-2/kg) of ^{125}I-$(Gal)_3$—IL-2 or ^{125}I-$(GalNAc)_3$—IL-2 into male mice (C57BL/6, 6w).

Antitumor Activity of IL-2 Derivatives

A subline from S908.D2-vp.2, which was originally selected from metastatic tumor cells in the regional lymph nodes of mice transplanted with the parental S908.D2 fibrosarcoma (13,14), was prepared by isolating the hepatic colonies of mice intrahepatically transplanted with S908.D2-vp.2, and was used for the murine hepatic tumor model. Briefly, 7.5×10^4 cells of the S908.D2-vp.2 subline were implanted intrahepatically into syngenic female mice (B10.D2, Sankyo Lab Service Co. Inc., Tokyo, Japan) on day 0. Seven days after tumor inoculation, $(Gal)_3$—IL-2, $(GalNAc)_3$—IL-2, unmodified IL-2, or saline was intravenously injected over 5 days (twice a day; high dose: 4.0×10^4 IL-2 unit/shot (150 μl), low dose: 1.0×10^4 IL-2 unit/shot (150 μl)). The therapeutic activity was evaluated by the tumor growth inhibition. The size of each tumor is represented as the product of the largest tumor diameter and the smallest tumor diameter (mm).

Preparation of Hepatocytes

Hepatocytes were prepared from male mice (C57BL/6, 4-8w) by a modified method of Seglen (15), and $4 \sim 6 \times 10^7$ cells, with viability of ≥90% as determined by trypan blue exclusion, were obtained from one liver perfusion. The monolayers were prepared by plating 1 mL containing 3×10^5 viable cells into twelve-well combination collagen (Type I)-coated plates (ASAHI Techno Glass Co., Tokyo, Japan). The hepatocytes were maintained in D-MEM containing 1% streptomycin/penicillin solution (v/v), 20 mM Hepes, and 10% heat-inactivated fetal bovine serum at 37°C in a humidified CO_2 incubator maintained at 95% air/5% CO_2 overnight. Protein concentrations were determined according to the Lowry method, using BSA as the standard.

In Vitro Binding Studies

Displacement of ^{125}I-ASOR binding to hepatocytes was determined by the modified method of Biessen *et al.* (16). In short, hepatocytes were incubated for 1 h at 4°C in 400 μl of DMEM containing 0.1% BSA with 0.6 nM of ^{125}I-ASOR in the presence or absence of $(Gal)_3$ or $(GalNAc)_3$ at 6 concentrations, ranging from 1 nM to 1 μM for $(GalNAc)_3$ and from 100 nM to 100 mM for $(Gal)_3$. After removing the medium by aspiration, the cells were washed four times with 1 ml of ice-cold D-PBS and were frozen at −80°C for 30 min or longer. The cells were dissolved in 0.75 ml of 0.1 M NaOH, and were counted to determine the binding counts in a γ-counter. The inhibition constants (K_i) were obtained by fitting the data to the following equation:

$$(C_{b(+I)} - \alpha)/(C_{b(-I)} - \alpha) = 1/(1 + I/K_i) \quad (1)$$

where $C_{b(+I)}/C_{b(-I)}$ represents the ratio of the binding in the presence of the ligand at its concentration of I to that in its absence. The α is the proportional constant for the non-saturable binding, which was fixed to the value obtained by fitting the binding of ^{125}I-ASOR in the presence of various concentrations of unlabeled ASOR to the Langmuir equation.

Pulse-Chase Experiments

The primary cultured mouse hepatocytes were incubated at 4°C for 2 h with 21 nM of ^{125}I-$(Gal)_3$—IL-2 and ^{125}I-$(GalNAc)_3$—IL-2 in 400 μL D-MEM in 12 well dishes. After three washes with ice-cold D-PBS, the cells were incubated at 37°C in D-MEM containing 0.1% BSA and 25 mM Hepes (pH 7.4) for the designated times. The reaction was stopped immediately by cooling on an ice-bath and transferring the supernatant to other tubes. A 150 μl aliquot of each supernatant was mixed with 150 μl of 20% TCA, allowed to stand for 10 min at 0°C, and centrifuged at 1000 g for 10 min. The radioactivities in the supernatant (degraded product, X_{deg}) and the pellet (the dissociated conjugates, L_{dis}) were separately counted. The cells were washed four times with 2 mL of ice-cold D-PBS, and were allowed to incubate twice in ice bath for 10 min with ice-cold D-PBS containing 20 mM EGTA (pH 5.0) to dissociate the cell surface-bound radioactivities (L_s). The cells were dissolved in 0.1 M NaOH to determine the internalized conjugates (L_i). The specific binding, internalized, dissociated, and degraded radioactivities were determined by subtracting the counts obtained in the pres-

ence of 100 mM GalNAc from those in its absence. Each amount with a bar represents the mean ± SD of triplicate measurements.

Continuous Incubation Studies

Hepatocytes were incubated at 37°C with 21 nM of ^{125}I-$(Gal)_3$—IL-2 or ^{125}I-$(GalNAc)_3$—IL-2 in 400 μL D-MEM containing 0.1% BSA and 25 mM Hepes (pH 7.4) for the designated times. The specific portions of L_s, L_i, and X_{deg} were determined as described for the pulse-chase experiments.

Kinetic Analysis of Receptor-Mediated Endocytosis (RME)

The mathematical model describing the RME process of the ligand—IL-2 conjugates was constructed by the method of Kuwabara *et al.* (17). In the pulse chase studies, both the internalization rate constant (k_{int}) and the dissociation rate constant (k_{off}) were calculated from the integration plots of the integrated amount of L_s vs L_i and L_{dis}, respectively (17). In the continuous incubation studies, the observed values for L_s, L_i, and X_{deg} were fitted to the following equations, respectively, to obtain k_{int}, k_{off}, k_{deg}, and $k_{on}R_T$:

$$dL_s/dt = k_{on}R_t\,C_e - (k_{off} + k_{int})\,L_s \quad (2)$$

$$dL_i/dt = k_{int}\,L_S - k_{deg}\,L_i \quad (3)$$

$$dX_{deg}/dt = k_{deg}\,L_i \quad (4)$$

where $k_{on}R_t$ and C_e are the association clearance of the ligand to the ASGP-R and the extracellular concentration, respectively. This fitting was performed using the nonlinear least squares method combined with the Runge Kutta Gill method, using the Napp program (18) with the ratio of k_{off} to k_{int} fixed to be equal to that obtained from the pulse chase study.

Simulation Study Using PBPK Model

Since the major organ for the distribution of ligand—IL-2 conjugates was the liver, the PBPK model simply consisted of the intracellular, surface, and extracellular spaces of the liver and the circulating plasma. The elimination pathways for the conjugates included RME in the liver and renal clearance. For the simulation of unmodified IL-2, an experimentally observed non-specific clearance in the liver was also considered. Hence, the mass balance equations for the concentration in circulating plasma (C_p) and C_e were expressed as:

$$dC_p/dt = (-Q_h\,C_p + Q_h\,C_e - CL_r\,C_p)/V_p \quad (5)$$

$$dC_e/dt = Q_h\,C_p - k_{on}R_t\,C_e\,F + k_{off}L_s - Q_h\,C_e - P_{nsp}\,F\,C_e)/V_e \quad (6)$$

where Q_h, CL_r, V_p, V_e, P_{nsp}, and F are hepatic plasma flow rate, renal clearance, distribution volume in circulating plasma, extracellular volume in the liver, nonspecific clearance for IL-2, and a scaling factor, respectively. Both Q_h and F were obtained by applying the observed values for CL_{uptake} and $k_{on}R_t$ of both ^{125}I-$(Gal)_3$—IL-2 and ^{125}I-$(GalNAc)_3$—IL-2 to the following equation:

$$CL_{uptake} = Q_h\,F\,k_{on}R_t/(Q_h + F\,k_{on}R_t) \quad (7)$$

This equation is based on the well-stirred model, where $k_{on}R_t$ was assumed to be the intrinsic clearance for CL_{uptake}. The V_p of the $(Gal)_3$—IL-2 and $(GalNAc)_3$—IL-2 was estimated by dividing the dose by the initial plasma concentration, which was obtained by fitting the plasma concentration profile to the monoexponential equation. The mass-balance equations for L_s, L_i, and X_{deg} of the ligand—IL-2 conjugates were Eq. (2), (3), and (4), respectively, whereas that for L_i of unmodified IL-2 was:

$$dL_i/dt = P_{nsp}\,C_e - k_{deg}\,L_i \quad (8)$$

where the k_{deg} was fixed to be the average of ^{125}I-$(Gal)_3$—IL-2 and ^{125}I-$(GalNAc)_3$—IL-2. The IL-2 receptor (IL-2R) occupancy in the liver was obtained by:

$$\text{Receptor occupancy} = C_e/(K_{d,IL\text{-}2} + C_e) \quad (9)$$

where $K_{d,IL\text{-}2}$ is the dissociation constant of IL-2R and is set to be 10 pM (19). The simulation was carried out by the Runge Kutta Gill method using STELLA II (High Performance Systems, Inc., Hanover, NH USA).

RESULTS

Characterization of the Ligands and Ligand—IL-2 Conjugates

Both $(Gal)_3$ and $(GalNAc)_3$ displayed monophasic inhibition of ^{125}I-ASOR binding to the mouse hepatocytes with the K_i of 191 ± 80 and 3.38 ± 0.42 nM, respectively, indicating ~50-fold higher affinity of $(GalNAc)_3$ than $(Gal)_3$. This result is in agreement with the previous reports (3,20) that indicated the higher binding affinity of GalNAc-terminated ligands for the ASGP-R than that of Gal-terminated ligands. The M-TGase-catalyzed conjugation of each ligand and IL-2 resulted in a 1:1 binding product that could be purified by reversed-phase HPLC. The recoveries of the $(Gal)_3$—IL-2 and $(GalNAc)_3$—IL-2 were 15.2 and 20.0%, respectively. The recoveries in terms of the IL-2 activity following the conjugation for $(Gal)_3$—IL-2 and $(GalNAc)_3$—IL-2 were 102% (9.21×10^6 IL-2 unit/mg) and 94% (8.45×10^6 IL-2 unit/mg), respectively. Thus, both conjugates retained biological activity almost equivalent to that of the unmodified IL-2.

Pharmacokinetics of $(Gal)_3$—IL-2 and $(GalNAc)_3$—IL-2

The liver concentrations of the two conjugates were much higher than that of IL-2, and the area under the hepatic concentration curve for $(GalNAc)_3$—IL-2 was about twice that of $(Gal)_3$—IL-2 (Fig. 1B). The disappearance of $(GalNAc)_3$—IL-2 from the circulation was, on the other hand, more rapid than that of $(Gal)_3$—IL-2, whereas IL-2 was the most stable in plasma (Fig. 1A). The CL_{uptake} of both conjugates was highest in the liver, followed by the kidney, and the CL_{uptake} in the liver of $(GalNAc)_3$—IL-2 was greater than that of $(Gal)_3$—IL-2 (Fig. 2).

Antitumor Effects of $(Gal)_3$—IL-2 and $(GalNAc)_3$—IL-2

Doses of 1×10^4 IL-2 U and 4×10^4 IL-2 U of $(Gal)_3$—IL-2 and 4×10^4 IL-2 U of IL-2 showed significant inhibition of S908.D2.vp2 sarcoma growth as compared to the control (Table I, $p < 0.05$). In contrast, neither dose of $(GalNAc)_3$—IL-2 yielded significant effects (Table I). The ratios of tumor-free mice after treatment with $(Gal)_3$—IL-2 were significantly

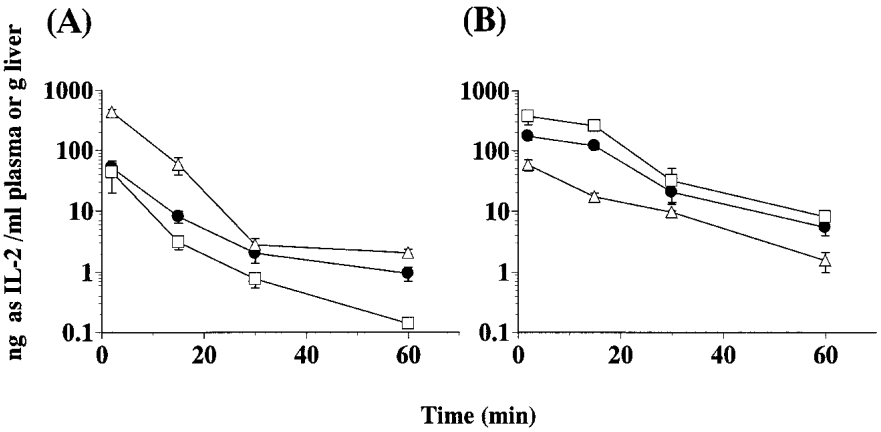

Fig. 1. Plasma concentration (A) and liver accumulation (B) of $(Gal)_3$—IL-2 (●), $(GalNAc)_3$—IL-2 (□), and IL-2 (△) following i.v. injection. Each protein was injected at a dose of 50 μg as IL-2/kg in male mice, and the concentrations both in plasma and liver were determined by ELISA. Each value represents the mean ± SD of three male mice (C57BL/6, 6w).

lower than those for the control, IL-2, and $(GalNAc)_3$—IL-2 groups at both doses. Thus, the antitumor potency was in the order of $(Gal)_3$—IL-2 > unmodified IL-2 > $(GalNAc)_3$—IL-2.

RME of ^{125}I-$(Gal)_3$—IL-2 and ^{125}I-$(GalNAc)_3$—IL-2 in Mouse Hepatocytes

In pulse chase studies the cell-surface bound ^{125}I-$(Gal)_3$—IL-2 was mainly dissociated in the medium, with a lower level of endocytosis whereas most of the ^{125}I-$(GalNAc)_3$—IL-2 was endocytosed into hepatocytes (Fig. 3). The integration plot revealed that the k_{int} values were 0.0340 and 0.0184 min^{-1}, whereas the k_{off} values were 0.0804 and 0.0118 min^{-1} for $(Gal)_3$—IL-2 and $(GalNAc)_3$—IL-2, respectively. During the continuous incubation, L_s of both conjugates rapidly reached the steady-state, whereas the L_i gradually increased and also reached a steady-state (Fig. 4). The X_{deg} increased after a lag time (~30 min, Fig. 4). These results exhibit the typical kinetic behavior in RME. Both the L_s and L_i values at a steady-state and the increase in X_{deg} were 4–8 fold higher for $(GalNAc)_3$—IL-2 than $(Gal)_3$—IL-2 (Fig. 4). The L_s of ^{125}I-IL-2 was negligible, whereas the L_i of ^{125}I-IL-2 was 28.1 ± 4.10 μl/mg protein at 240 min (data not shown). By model fitting, a remarkable difference was observed in the k_{off} between the two conjugates (Table II). The k_{off}/k_{int} was 2.3 for $(Gal)_3$—IL-2 and 0.63 for $(GalNAc)_3$—IL-2. Thus, $(Gal)_3$—IL-2 avoided endocytosis, as compared with $(GalNAc)_3$—IL-2.

Simulation of the Concentration Profiles of the Conjugates Based on a PBPK Model

To explain the difference in the antitumor effects among the conjugates and the unmodified IL-2, simulation studies were performed using parameters listed in Table III, most of which were obtained either from *in vitro* or *in vivo* studies, or are cited from the references. Since both conjugates exhibit

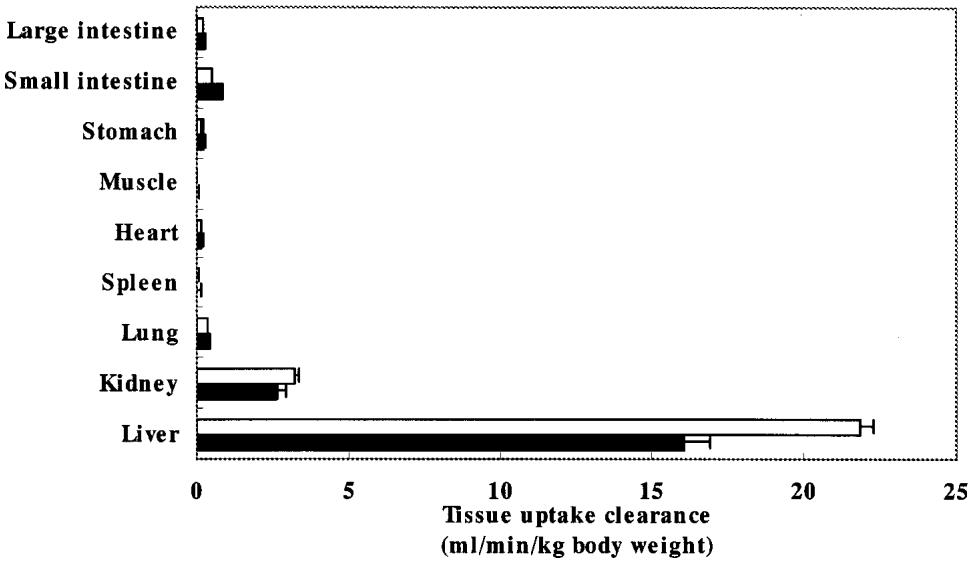

Fig. 2. Tissue uptake clearance of ^{125}I-$(Gal)_3$—IL-2 (■) and ^{125}I-$(GalNAc)_3$—IL-2 (□). ^{125}I-modified ligand—IL-2 conjugates were intravenously injected at a dose of 50 μg as IL-2/kg in male mice, and the plasma concentration profile up to 3 min and the tissue concentration at 3 min of the radioactivity were determined. Each value represents the mean ± SD of three or four mate mice (C57BL/6, 6w).

Table I. Residual Tumor Sizes in Mice after Repeated i.v. Administrations of $(Gal)_3$-IL-2, $(GalNAc)_3$-IL-2, or IL-2 in the Hepatic Tumor Model

Treatment	Dose (U/shot)	N	Tumor volume		Number of tumor free mouse
			Mean (mm)	Actual values (mm)	
Saline	–	5[a]	6.83 ± 5.32	3.07, 3.45, 9.96, 14.74, 2.92	0/5
IL-2	1×10^{-4}	7	1.60 ± 0.39	1.33, 2.08, 2.18, 1.20, 1.30, 1.45, 1.67	0/7
IL-2	4×10^{-4}	6[a]	1.55 ± 1.18[b]	0.00, 1.67, 3.63, 1.49, 1.32, 1.21	0/6
$(Gal)_3$-IL-2	1×10^{-4}	7	0.65 ± 1.01[b]	2.73, 0.00, 0.86, 0.00, 0.95, 0.00, 0.00	4/7[c]
$(Gal)_3$-IL-2	4×10^{-4}	7	0.53 ± 0.91[b]	1.68, 0.00, 0.00, 0.00, 0.00, 0.00, 2.02	5/7[c]
$(GalNAc)_3$-IL-2	1×10^{-4}	7	3.72 ± 5.61	1.53, 1.71, 2.18, 1.61, 16.41, 1.33, 1.23	0/7
$(GalNAc)_3$-IL-2	4×10^{-4}	6[a]	3.86 ± 4.54	12.91, 1.42, 1.03, 2.54, 3.75, 1.52	0/6

The S908.D2.vp2 sarcoma was implanted intrahepatically into female mice (B10D2, 6w) on day 0 (n = 7). Seven days after the implantation, modified and unmodified IL-2 were intravenously injected twice a day.

[a] One or two mice died before the end of the experiment.

[b] $P < 0.05$ as compared to control (Dunnett's-*t*-test).

[c] $P < 0.01$ as compared to control, IL-2, and $(GalNAc)_3$-IL-2 (Fisher's protected LSD).

similar biological activity to IL-2, the $K_{d,IL\text{-}2}$ value was set to be equal for the three compounds. Since the two conjugates exhibited comparable V_p, k_{deg} (Table III), and CL_{uptake} values in the kidney (Fig. 2), the means of those values were used for the simulation of IL-2 disposition.

Although the absolute values simulated (Fig. 5) were different from those experimentally observed (Fig. 1), the simulated hepatic accumulations of $(Gal)_3$—IL-2 and $(GalNAc)_3$—IL-2 were much higher than that of IL-2, with that of $(Gal)_3$-IL-2 being slightly higher than that of $(GalNAc)_3$—IL-2 during the initial period (Fig. 5B). The $(GalNAc)_3$—IL-2 in plasma rapidly decreased, whereas IL-2 was most stable, at least in the initial phase (Fig. 5A). The simulated IL-2R occupancy in the liver rapidly decreased after the injection of $(GalNAc)_3$—IL-2, whereas the relatively higher IL-2R occupancy (>80%) was maintained for a longer period after the injection of $(Gal)_3$—IL-2 (Fig. 5C). To examine the optimal combination of k_{off} and k_{int}, the IL-2 concentration profile in the hepatic extracellular space, which should directly reflect the exposure of IL-2 to the effector cells (pharmacological target of IL-2), and the IL-2R occupancy in the liver were simulated by varying k_{int} when the k_{off} and other parameters were kept constant to that for $(Gal)_3$—IL-2 (0.209 min^{-1}). The lower k_{int} value resulted in longer exposure of IL-2 in the extracellular space and greater IL-2R occupancy in this case (Fig. 6A, 6B). On the other hand, Fig. 6C and 6D, and Fig. 6E and 6F show the simulated profiles of IL-2 when the k_{int} was set to the constant value of $(Gal)_3$—IL-2 (0.0896 min^{-1}) and at much lower value (0.000896 min^{-1}) (3), respectively. In Fig. 6C, the longer exposure of IL-2 in the hepatic extracellular space was obtained at the higher k_{off} value, possibly due to its lower affinity to ASGP-R and slower receptor-mediated clearance. The IL-2R occupancy (Fig. 6D) was, therefore, higher at the higher k_{off} value, although slope of the curve for IL-2R occupancy in Fig. 6D was sharper, as compared with that at the optimal (k_{int} ~ 0.000896 min^{-1}) condition in Fig. 6B. In Fig. 6E, the larger k_{off} value resulted in the higher extracellular concentration during the initial period, which was followed by its rapid decrease, whereas the lower k_{off} exhibited the rapid decrease during the initial period, which was followed by the maintained concentration. Therefore, the IL-2R occupancy at the k_{off} value of 0.209 min^{-1} was maintained at a higher level (>99%) for a longer time period (Fig. 6F). Thus, there seems to be an optimal k_{off} value for longer exposure to the IL-2R, and the k_{off}/k_{int} ratio affects the targeting efficacy of the ligand to ASGP-R.

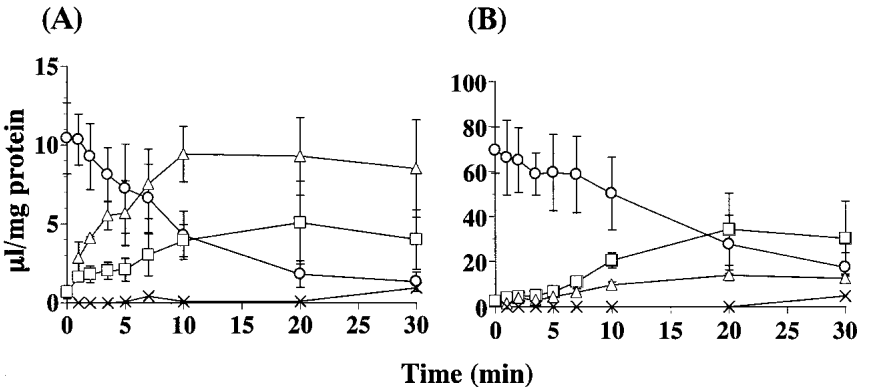

Fig. 3. Fate of cell-surface bound ^{125}I-$(Gal)_3$—IL-2 (A) and ^{125}I-$(GalNAc)_3$—IL-2 (B) in primary cultures of mouse hepatocytes (Pulse-chase studies). ^{125}I-modified IL-2 was bound to cells at 4°C for 2 h. After washing, the cells were transferred to ligand-free medium and were incubated at 37°C. The surface-bound (○), internalized (□), and dissociated (△) radioactivity, and degradation product (×) were determined. Each value represents the mean ± SD of three experiments.

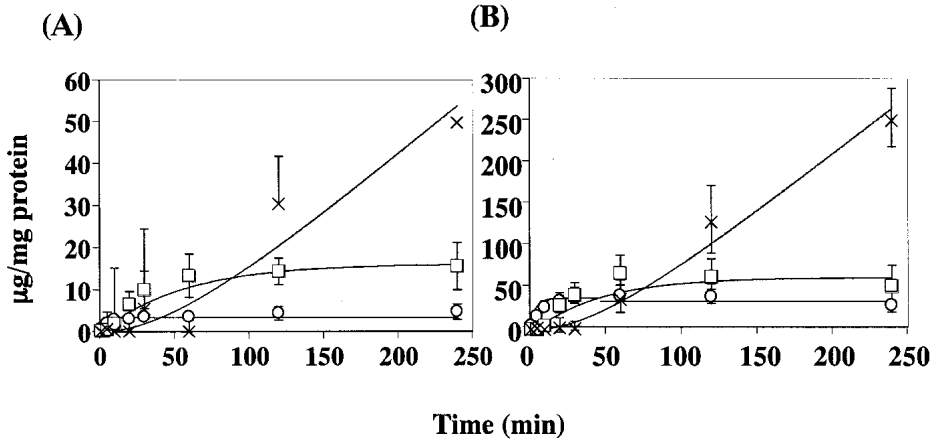

Fig. 4. Time course of cell-associated radioactivity and degradation products during continuous incubations with ^{125}I-$(Gal)_3$—IL-2 (A) and ^{125}I-$(GalNAc)_3$—IL-2 (B) in primary cultured mouse hepatocytes. The cells were incubated with ^{125}I-ligand—IL-2 conjugates at 37°C for various time periods. Surface-bound (○), internalized (□), and degraded (×) amounts were counted. Each value represents the mean ± SD of triplicate measurements. The straight lines indicate the simulated values obtained by model fitting.

DISCUSSION

This study was designed to evaluate the targeting efficiency of the $(Gal)_3$-mediated hepatic delivery of IL-2 via ASGP-R. By comparing the kinetic profiles of the binding and the internalization between $(Gal)_3$—IL-2 and $(GalNAc)_3$—IL-2 (Figs. 3 and 4, Table I), we demonstrated that the $(Gal)_3$ ligand has a special feature that allows it to avoid ASGP-R-mediated endocytosis, and to be targeted specifically to the liver after binding to the ASGP-R on hepatocytes.

In the S908.D2.vp2 tumor model, the antitumor efficacy of $(Gal)_3$—IL-2 was found to be superior to those of unmodified IL-2 and $(GalNAc)_3$—IL-2 (Table I). The S908.D2.vp2 murine sarcoma model was chosen in this study, since this is one of the most sensitive models to IL-2 therapy (13,14). This may be appropriate for demonstrating the differences in the antitumor potential of each protein. In this model, the antitumor effect of IL-2 against established S908.D2 sarcoma was reported to be mediated by CD8+ CTL cells, which directly mediate tumor cell killing, rather than anomalous killer cells such as NK and LAK cells. This result suggests that the binding of IL-2 to its receptor on the CD8+ CTL cells in the liver is the critical factor determining the antitumor activity. In fact, a genetically engineered fusion protein consisting of a human/mouse chimeric anti-ganglioside GD2 antibody and recombinant human interleukin 2 could specifically target IL-2 to tumor sites via the recognition of ganglioside by antibody, and effectively stimulate immune effector cells (21). Although there has been no direct demonstration for the importance of IL-2 receptor occupancy as a critical factor de-

Table II. Kinetic Parameters for the Receptor-Mediated Endocytosis of ^{125}I-$(Gal)_3$-IL-2 and $(GalNAc)_3$-IL-2 in Primary Cultured Mouse Hepatocytes

	k_{int} (min^{-1})	k_{off} (min^{-1})	k_{deg} (min^{-1})	$k_{on}R_t$/min/mg
$(Gal)_3$-IL-2	0.0896	0.209	0.0183	0.986
(SD)		(0.0806)	(0.0023)	(0.0520)
$(GalNAc)_3$-IL-2	0.0451	0.0286	0.0232	2.43
(SD)		(0.0053)	(0.0029)	(0.107)

Table III. The Parameters Used in Simulation Studies

Parameters	Definition	Values
$k_{on}R_t$	Association clearance of the ligand to the receptor	0.986 μl/min/mg (Gal)[a] 2.43 μl/min/mg (GalNAc)[a] 0 μl/min/mg (IL-2)[a]
k_{off}	Dissociation rate constant of the ligand	0.209/min (Gal)[a] 0.0286/min (GalNAc)[a]
k_{int}	Internalization rate constant of the ligand	0.0896/min (Gal)[a] 0.0451/min (GalNAc)[a]
k_{deg}	Degradation rate constant of the internalized ligand	0.0183/min (Gal)[a] 0.0232/min(GalNAc)[a] 0.0208/min (IL-2)[c]
F	Scaling factor from *in vitro* to *in vivo*	36.9 mg/g body weight[b]
V_p	Distribution volume in plasma	40.1 ml/kg (Gal)[b] 29.9 ml/kg (GalNAc)[b] 35.0 ml/kg (IL-2)[c]
V_e	Volume of extracellular space in the liver	11.8 ml/kg (28)
Q_H	Hepatic plasma flow rate	28.5 ml/min/kg[b]
CL_r	Renal clearance	2.64 ml/min/kg (Gal)[b] 3.24 ml/min/kg (GalNAc)[b] 2.94 ml/min/kg (IL-2)[c]
P_{nsp}	Nonspecific clearance in the liver	0.117 μl/min/mg (IL-2)[a]
Dose	Dose of ligand-IL-2 conjugate	5×10^4 ng/kg
Kd_{IL-2}	Dissociation constant for IL-2 receptor	0.155 ng/ml

[a] Parameters obtained from *in vitro* studies.
[b] Parameters from *in vivo* studies.
[c] Average value between $(Gal)_3$-IL-2 and $(GalNAc)_3$-IL-2.

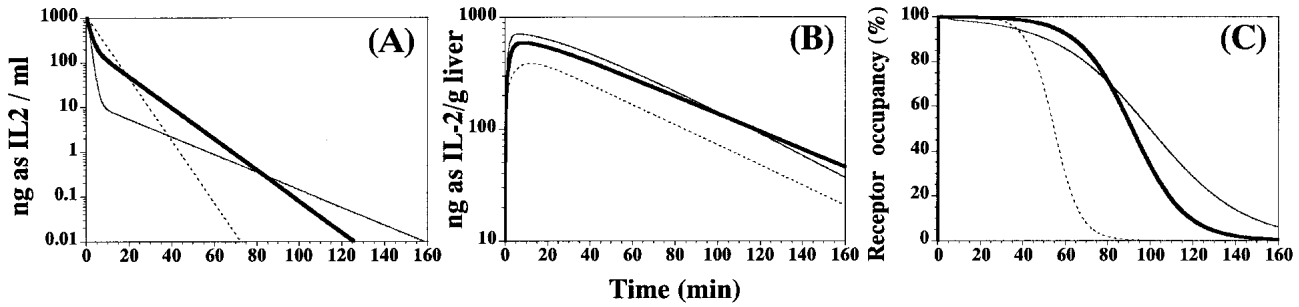

Fig. 5. The simulation for the time profile of the concentration in plasma (A) and liver (B), and the IL-2R occupancy in the liver (C) after intravenous administration of $(Gal)_3$—IL-2 (bold line), $(GalNAc)_3$—IL-2 (thin line), and unmodified IL-2 (dotted line). The simulation was performed based on the PBPK model, using the parameters listed in Table 3.

termining the antitumor activity, we performed the simulation study for such occupancy to quantify the degree of the receptor binding of IL-2.

In addition to its higher pharmacological activity, $(Gal)_3$—IL-2 is specifically targeted to the liver (Fig. 2). In our preliminary studies, the wet organ weight of the lung, assessed as the toxicity exerted by IL-2, was significantly increased by IL-2 (40 μg/day), but not by $(Gal)_3$—IL-2, whereas that of the liver was increased by the same dose of $(Gal)_3$—IL-2 and IL-2. These results suggest the efficient hepatic-targeting and the site-selective delivery of IL-2 by incorporating $(Gal)_3$. Since high systemic doses of IL-2 cause severe side-effects, including capillary leak syndrome especially in the lung, the hepatic-targeting of IL-2 should be useful for delivering an increased amount of IL-2 near the tumor microenvironment in the liver, while decreasing the IL-2 delivery and toxicity to other organs (22,23).

The highest distribution to the liver was observed for $(GalNAc)_3$—IL-2 (Fig. 1), which had the lowest antitumor potential (Table I). This higher hepatic distribution of $(GalNAc)_3$—IL-2 was also confirmed by the higher CL_{uptake} of $(GalNAc)_3$—IL-2 in the liver (Fig. 2). However, the plasma disappearance of $(GalNAc)_3$—IL-2 was the most rapid (Fig. 1). Thus, the higher hepatic distribution results in the higher systemic elimination of this ligand. It should be noted that the hepatic distribution assessed *in vivo* includes the ligands that

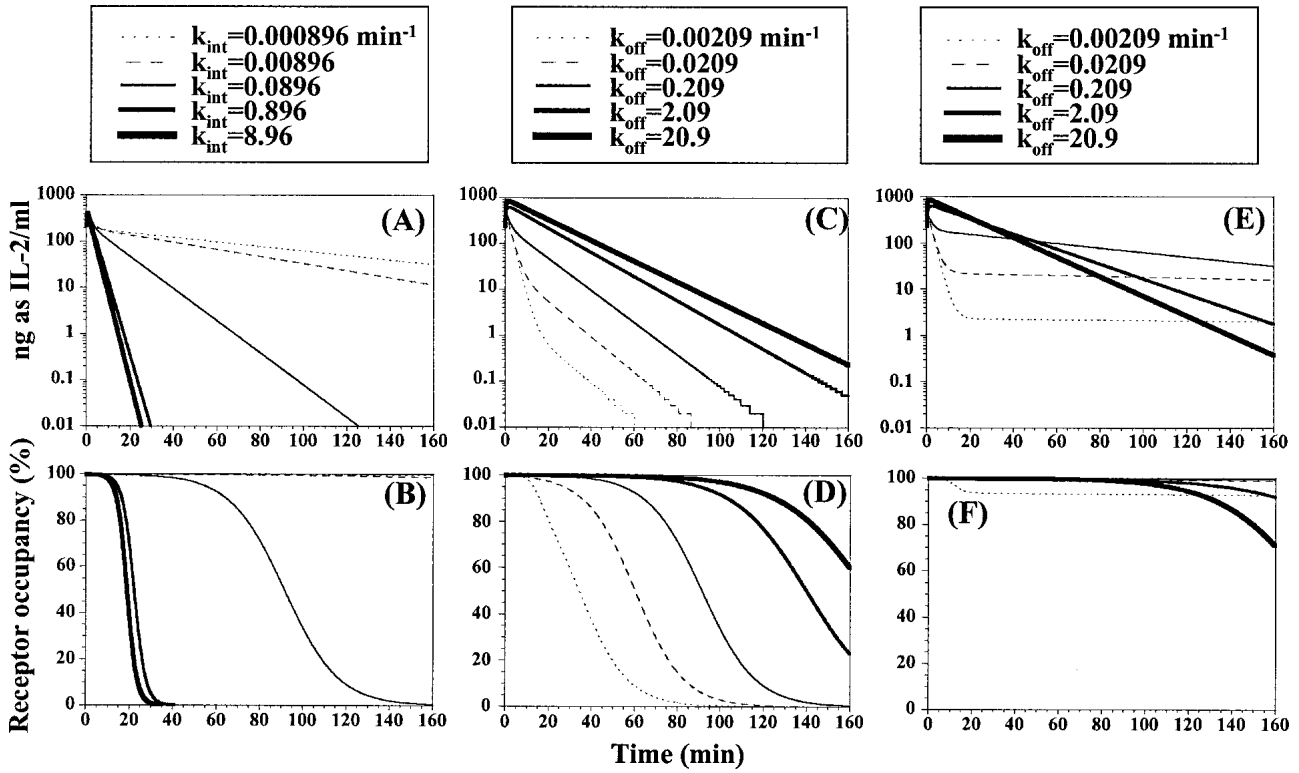

Fig. 6. The simulation for the time profile of IL-2 concentration in the hepatic extracellular space (A, C, E) and IL-2R occupancy in the liver (B, D, F) after the intravenous administration of the ligand—IL-2 conjugate. In panel A and B, the k_{off} value was set to be that of $(Gal)_3$—IL-2 (0.209 min^{-1}), whereas the k_{int} value was varied between 100 and 1/100 times that of $(Gal)_3$—IL-2. In panels C and D, the k_{int} value was set to be that of $(Gal)_3$—IL-2 (0.0896 min^{-1}), whereas the k_{off} value was varied between 100 and 1/100 times that of $(Gal)_3$—IL-2. In panels E and F, the k_{int} value was set to be 1/100 that of $(Gal)_3$—IL-2 (0.000896 min^{-1}), whereas the k_{off} value was varied between 100 and 1/100 times that of $(Gal)_3$—IL-2. All the other parameters were set to be those of $(Gal)_3$—IL-2. In panel F, the data at the k_{off} value of 0.209 min^{-1} were almost superimposable onto those at the k_{off} value of 0.0209 min^{-1}, and were simulated to be more than 99% until 160 min.

are present in the extracellular space, associated on the cell-surface, and endocytosed into the cells. Therefore, further kinetic analyses are needed to clarify the difference in the hepatic disposition between each ligand (Figs. 3, 4). The pulse-chase study in mouse hepatocytes revealed that the k_{off} value of $(Gal)_3$—IL-2 was much higher than that of $(GalNAc)_3$—IL-2 (Table I). Additionally, $(Gal)_3$—IL-2 showed a much higher K_i value than that of $(GalNAc)_3$—IL-2 (see Results). Therefore, $(Gal)_3$—IL-2 has a lower affinity for ASGP-R and can be more easily dissociated from the cell-surface receptor after the binding, thus avoiding receptor-mediated internalization and subsequent intracellular degradation.

Considering the difference in the kinetic parameters of $(Gal)_3$—IL-2 and $(GalNAc)_3$—IL-2, the higher affinity to ASGP-R does not necessarily result in the higher pharmacological potential of IL-2. To examine our hypothesis that there might be on optimal affinity of the ligand for delivering IL-2 to the effector cells, simulation studies based on the PBPK model were carried out (Figs. 5 and 6, Table III). Although further studies are needed to construct a PBPK model with higher compatibility with the experimentally observed absolute values, the present PBPK model principally reproduces the pharmacokinetic property of each ligand in terms of: (i) The disappearance from circulating plasma was in the order of $(GalNAc)_3$—IL-2 > $(Gal)_3$—IL-2 > IL-2, indicating that $(Gal)_3$ has moderate stability in the systemic circulation among the three proteins. (ii) The hepatic IL-2 concentration was in the order of $(GalNAc)_3$—IL-2 > $(Gal)_3$—IL-2 >> IL-2, suggesting that $(Gal)_3$ exhibits a moderate hepatic distribution. (iii) The residence time for IL-2R occupation (>80%) was in the order of $(Gal)_3$—IL-2 > IL-2 > $(GalNAc)_3$—IL-2, which was consistent with the antitumor potency in the hepatic tumor model (Table I).

Based on the PBPK model thus constructed, both the pharmacokinetic profiles and the IL-2R occupancy of ligand—IL-2 conjugates with various pharmacokinetic properties can be simulated. Therefore, further simulation studies were performed to identify the conjugate with the optimal kinetic parameters for increasing the pharmacological potential (Fig. 6). The following two points seemed to be the important for delivering the conjugate to the hepatic extracellular space. First, the k_{int} value should be as small as possible. When the k_{int} value was set to be at less than that of $(Gal)_3$—IL-2, the simulated conjugate concentration in the hepatic extracellular space and the IL-2R occupancy in the liver were higher, as the k_{int} value was lower (Fig. 6A,B). Since the k_{int} value represents the intrinsic efficacy for endocytosis in hepatocytes, it is reasonable for the ligand with a lower k_{int} to circulate for a longer period by avoiding internalization. Second, the k_{off}/k_{int} should be important since the higher k_{off}/k_{int} indicates the higher stability of the conjugate in the circulation due to endocytosis avoidance (Fig. 6C–6F). Nevertheless, if this ratio greatly exceeds that of the optimal condition, then the ligand—IL-2 conjugate cannot be retained for a longer time, due to the low affinity for the ASGP-R. When the k_{int} was set to a much lower value than that of $(Gal)_3$—IL-2 (Fig. 6F), the simulated IL-2R occupancy was highest, with values up to 160 min at k_{off} of $(Gal)_3$—IL-2 (Fig. 6F). These results suggest that the balance between the two parameters (k_{int} and k_{off}) is important to produce the higher pharmacological activity of IL-2.

As well as the ASGP-R on hepatocytes, galactose particle receptor on Kupper cells can also mediate the uptake of galactose-exposing particles. However, the effect of these receptors for the pharmacokinetics and pharmacodynamic profiles of $(Gal)_3$—IL-2 or $(GalNAc)_3$—IL-2 would be small because of the following reasons. It is reported that high affinity recognition of ^{125}I-asialofetuin (competed for by an excess of unlabelled asialofetuin) is exerted by hepatocytes, not by Kupper cells, after intravenous injections in rats (24). Furthermore, Kupper cells are unable to internalize small galactose-terminated molecules such as asialofetuin via their galactose particle receptors. These results indicate that galactose-terminated ligand has minimal specific affinity for galactose-particle receptor on Kupper cells. In fact, hepatic targeting of both $(Gal)_3$ and $(GalNAc)_3$ ligands in the liver of mice was similarly decreased by coadministering asialofetuin (data not shown). $(Gal)_3$—IL-2 was also targeted to the liver in mice, but competed by asialoorosomucoid (7). Considering also that the number of Kupper cells is much smaller (about 1/10) than that of hepatocytes in the liver, it is concluded that the hepatic targeting of $(Gal)_3$—IL-2 and $(GalNAc)_3$—IL-2 is mediated mainly by ASGP-R binding on hepatocytes.

Although $(Gal)_3$ and $(Gal)_3$—IL-2 had much lower affinity (higher K_i and koff) to ASGP-R than $(GalNAc)_3$ and $(GalNAc)_3$—IL-2, the difference in the hepatic distributions between the two conjugates was not so obvious (Figs. 1, 2). This result can be explained if we consider that the hepatic association of these two conjugates was closely limited by the plasma flow rate, since the CL_{uptake} of $(Gal)_3$—IL-2 and $(GalNAc)_3$—IL-2 (Fig. 2) was not very different from Q_h (Table III). Therefore, it is reasonable that the change in the intrinsic affinity to ASGP-R does not proportionally affect the hepatic targeting observed *in vivo*.

Our hepatic targeting system using $(Gal)_3$ is a novel and attractive methodology for therapeutic protein treatment of liver diseases, since this system can deliver cytokines to the extracellular space in the liver, where the pharmacologic action takes place. In fact, the antitumor effect of IL-2 seemed to be increased by this system (Table I). As compared with the previous hepatic delivery systems, which randomly derivatize the proteins with oligosaccharide moieties or modify the carbohydrate chains of the native proteins, this methodology is useful in terms of the following points: (i) We can design a variety of ligands to achieve favorable pharmacokinetic properties for each therapeutic protein. (ii) The constructed conjugate in this methodology has a homologous structure with a single site of $(Gal)_3$ incorporation (7). The concept that the lower affinity to ASGP-R may produce higher pharmacological activity might be applicable to delivery systems to other types of receptors that are highly expressed on specific cells, like the case of ASGP-R. Mannose receptor would be another target for delivering proteins around non-parenchymal cells, because of its higher expression in those cells (25). Since higher transferrin receptor and folate receptor expression is observed on carcinoma cells as compared to normal cells, these might be attractive targets for specific delivery to the tumor (26,27). Our methodology would also be applicable to a variety of therapeutic proteins for their hepatic delivery. However, the relationship between the structures and the properties to the ASGP-R of the ligands is the next problem to be solved.

In conclusion, the hepatic targeting system utilizing the

$(Gal)_3$ ligand shows great potential for future therapeutic applications of protein drugs. To improve the targeting efficacy, the kinetic properties avoiding endocytosis are important, including the affinity to ASGP-R, the absolute value of k_{int}, and the ratio of k_{off} to k_{int}.

ACKNOWLEDGMENTS

This work was carried out under the support of Drug Delivery System Institute, Ltd. We are grateful to Dr. Hiroyuki Ishihara (Eisai Co., Ltd.) for his advice concerning preparation of hepatocytes. We are also very indebted to Dr. Miroslav Smriga (Ajinomoto Co., Inc.) for critical reading of the manuscript and helpful suggestions.

REFERENCES

1. G. Ashwell and J. Harford. Carbohydrate-specific receptors of the liver. *Annu. Rev. Biochem.* **51**:531–554 (1982).
2. M. Spiess. The asialoglycoprotein receptor: a model for endocytic transport receptors. *Biochemistry* **29**:10009–10018 (1990).
3. Y. C. Lee, R. R. Townsend, M. R. Hardy, J. Lonngren, J. Arnarp, M. Haraldsson, and H. Lonn. Binding of synthetic oligosaccharides to the hepatic Gal/(GalNAc) lectin. Dependence on fine structural features. *J. Biol. Chem.* **258**:199–202 (1983).
4. R. T. Lee, P. Lin, and Y. C. Lee. New synthetic cluster ligands for galactose/N-acetylgalactosamine-specific lectin of mammalian liver. *Biochemistry* **23**:4255–4261 (1984).
5. K. Kasama, J. Utsumi, E. Matsuo–Ogawa, T. Nagahata, Y. Kagawa, S. Yamazaki, and Y. Satoh. Pharmacokinetics and biologic activities of human native and asialointerferon-beta s. *J. Interferon Cytokine Res.* **15**:407–415 (1995).
6. Y. Yabe, M. Nishikawa, A. Tamada, Y. Takakura, and M. Hashida. Targeted delivery and improved therapeutic potential of catalase by chemical modification: combination with superoxide dismutase derivatives. *J. Pharmacol. Exp. Ther.* **289**:1176–1184 (1999).
7. H. Sato, E. Hayashi, N. Yamada, M. Yatagai, and Y. Takahara. Further studies on the site-specific protein modification by microbial transglutaminase. *Bioconjug. Chem.* **12**:701–710 (2001).
8. T. Tsuji, R. Nakagawa, N. Sugimoto, and K. Fukuhara. Characterization of disulfide bonds in recombinant proteins: reduced human interleukin 2 in inclusion bodies and its oxidative refolding. *Biochemistry* **246**:3129–3134 (1987).
9. M. D. Bider, R. Cescato, P. Jeno, and M. Spiess. High-affinity ligand binding to subunit H1 of the asialoglycoprotein receptor in the absence of subunit H2. *Eur. J. Biochem.* **230**:207–212 (1995).
10. H. Sato, Y. Takahara, E. Hayashi, M. Yatagai, M. Suzuki, T. Tabata, and C. Ejima. Modified physiologically active protein and pharmaceutical composition containing the same. P.C.T. JP97/03435.
11. S. Gillis, M. M. Ferm, W. Ou, and K. A. Smith. T cell growth factor: parameters of production and a quantitative microassay for activity. *J. Immunol.* **120**:2027–2032 (1978).
12. F. Greenwoon, W. Hunter, and J. Glover. The preparation of ^{131}I-labeled human growth hormone of high specific activity. *Biochem. J.* **89**:114–123 (1963).
13. J. Hamuro, T. Kikuchi, F. Takatsuki, and M. Suzuki. Cancer cell progression and chemoimmunotherapy—dual effects in the induction of resistance to therapy. *Br. J. Cancer* **73**:465–471 (1996).
14. M. Suzuki, T. Kikuchi, F. Takatsuki, and J. Hamuro. Curative effects of combination therapy with lentinan and interleukin-2 against established murine tumors, and the role of CD8-positive T cells. *Cancer Immunol. Immunother.* **38**:1–8 (1994).
15. P. O. Seglen. Hepatocyte suspensions and cultures as tools in experimental carcinogenesis. *J. Toxicol. Environ. Health* **5**:551–560 (1979).
16. E. A. Biessen, D. M. Beuting, H. C. Roelen, G. A. van de Marel, J. H. van Boom, and T. J. van Berkel. Synthesis of cluster galactosides with high affinity for the hepatic asialoglycoprotein receptor. *J. Med. Chem.* **38**:1538–1546 (1995).
17. T. Kuwabara, S. Kobayashi, and Y. Sugiyama. Kinetic analysis of receptor-mediated endocytosis of G-CSF derivative, nartograstim, in rat bone marrow cells. *Am. J. Physiol.* **271**:E73–84 (1996).
18. A. Hisaka, and Y. Sugiyama. Analysis of nonlinear and nonsteady state hepatic extraction with the dispersion model using the finite difference method. *J. Pharmacokinet. Biopharm.* **26**:495–519 (1998).
19. G. Ju, L. Collins, K. L. Kaffka, W. H. Tsien, R. Chizzonite, R. Crowl, R. Bhatt, and P. L. Kilian. Structure-function analysis of human interleukin-2. Identification of amino acid residues required for biological activity. *J. Biol Chem.* **262**:5723–5731 (1987).
20. R. R. Townsend, M. R. Hardy, T. C. Wong, and Y. C. Lee. Binding of N-linked bovine fetuin glycopeptides to isolated rabbit hepatocytes: Gal/GalNAc hepatic lectin discrimination between Gal beta(1,4)GlcNAc and Gal beta(1,3)GlcNAc in a triantennary structure. *Biochemistry* **25**:5716–5725 (1986).
21. H. S. Sabzevari, S. D. Gllies, B. M. Mueller, and J. D. Pancook. A recombinant antibody-interleukin 2 fusion protein suppresses growth of hepatic human neuroblastoma metastases in severe combined immunodeficiency mice. *Proc. Natl. Acad. Sci. USA* **91**:9626–9630 (1994).
22. H. Abdih, C. J. Kelly, D. Bouchier-Hayes, M. Barry, and S. Kearns. Taurine prevents interleukin-2-induced acute lung injury in rats. *Eur. Surg. Res.* **32**:347–352 (2000).
23. H. Mann, J. H. Ward, and W. E. Samlowski. Vascular leak syndrome associated with interleukin-2: chest radiographic manifestations. *Radiology* **176**:191–194 (1990).
24. T. J. C. van Berkel, C. J. Dekker, J. K. Kruijt, and H. G. van Eijk. The interaction in vivo of transferrin and asialotransferrin with liver cells. *Biochem. J.* **243**:715–722 (1987).
25. Y. Takakura, S. Masuda, H. Tokuda, M. Nishikawa, and M. Hashida. Targeted delivery of superoxide dismutase to macrophages via mannose receptor-mediated mechanism. *Biochem. Pharmacol.* **47**:853–858 (1994).
26. R. J. Lee and P. S. Low. Delivery of liposomes into cultured KB cells via folate receptor-mediated endocytosis. *J. Biol. Chem.* **269**:3198–3204 (1994).
27. S. P. Vyas, A. Singh, and V. Sihorkar. Ligand-receptor-mediated drug delivery: an emerging paradigm in cellular drug targeting. *Crit. Rev. Ther. Drug Carrier Syst.* **18**:1–76 (2001).
28. R. L. Dedrick, D. D. Forrester, J. N. Cannon, S. M. el-Dareer, L. B. Mellett. Pharmacokinetics of 1-b-D-arbino-furanosylcytocine (Ara-C) deamination in several species. *Biochem. Pharmacol.* **22**:2405–2417 (1973).